Evaluation of Grasp Force Efficiency Considering Hand Configuration and Using Novel Generalized Penetration Distance Algorithm

Yu Zheng and Katsu Yamane

***Abstract*— This paper proposes a new grasp force efficiency (GFE) measure that considers not only contact point locations but also the hand configuration and mechanism. GFE evaluates the largest wrench applied to the object that the grasp can resist with unit contact forces. Traditional GFE measures depend solely on the contact point locations without considering how the unit contact forces are generated. Intuitively, however, the actuators' effort required to generate unit contact forces depends on the hand configuration and mechanism and therefore should affect the grasp efficiency. For example, generating a unit contact force with an under-actuated finger would be more difficult than with a fully actuated finger. Our new GFE measure addresses this issue and is potentially useful for hand mechanism design as well as grasp planning.**

We also present a novel geometry-based iterative algorithm for computing the generalized penetration distance of a point in an arbitrary convex set. The algorithm allows unified and accurate computation of the new and traditional GFE measures with various criteria without linear approximation. Other applications of the algorithm include penetration depth computation of two convex objects for physics simulation.

I. Introduction

Fair and quick evaluation of grasp quality is a critical element in grasp planning algorithms. Readers are referred to [1] for a summary of existing grasp quality measures. A grasp quality measure that is often used in grasp planning [2]–[6] evaluates the minimum of the largest wrench applied to the object that the grasp can resist with unit contact forces, and it gives the "efficiency" of a grasp [7], [8]. To distinguish it from other grasp quality measures mentioned in [1], we call it the grasp force efficiency (GFE) measure. Geometrically, GFE is equivalent to the radius of the largest origin-centered ball contained, or the penetration distance of the origin, in the grasp wrench set (GWS). GWS is defined as the convex hull of either the union or the Minkowski sum of primitive contact wrenches [8].

This measure has two issues. First, traditional GFE measures depend solely on the contact point locations on the object without considering how the unit contact forces are generated. Intuitively, however, the actuators' effort required to generate unit contact forces depend on the hand configuration and mechanism, and therefore should affect the grasp efficiency. For example, generating a unit contact force with an under-actuated finger would generally be more difficult than with a fully actuated finger. Recently some researchers considered the hand configurations in grasp planning [3], [5] but they used a GFE measure that does not consider the hand configuration. Ceccarelli [9] used another GFE defined as the ratio of the squeezing force on fingertips to the force exerted by the actuator and applied it to two-finger, one-actuator gripper design. However, it is not clear how to extend this measure to general robot hands.

Second, accurate and efficient computation of the GFE is always difficult because the penetration distance usually has many local minima. A workaround is to approximate the friction cone by a polygonal pyramid such that the GWS becomes a polytope and the minimum distance from the origin to its facets approximates the penetration distance [10]. Borst et al. [11] incrementally refined the polygonal pyramid that approximates the friction cone to mitigate the inaccuracy due to linearization. Zhu and Wang [2] replaced the ball by a polytope and only computed the largest wrenches in the directions of polytope's vertices, so that the computation can be reduced to a set of linear programs. However, these methods still suffer from efficiency and/or accuracy issues.

In this paper, we first propose a novel GFE measure that considers the hand properties that affect the grasp efficiency, such as the finger poses and actuator placements. The new GFE measure is derived by computing the GWS that includes only the wrenches generated by joint torques, where we take into account the hand configuration and actuator placements. It is therefore useful not only for grasp planning but also for hand mechanism design.

We then present a novel geometry-based algorithm for computing the generalized penetration distance of a point in an arbitrary convex set, which allows unified and accurate computation of both new and existing GFE measures with various criteria without linear approximation. While this paper uses this algorithm specifically for GFE measure computation, it is also applicable to other applications of penetration distance including contact force optimization for grasping [12]–[14] and penetration depth computation between two convex objects for physics simulation.

II. Grasp Force Efficiency (GFE) Measure

Consider a robot hand grasping an object at m contact points as shown in Fig. 2a. Let $\boldsymbol{p}_i$, $\boldsymbol{n}_i$, $\boldsymbol{o}_i$ and $\boldsymbol{t}_i$ be the position, the unit inward normal, and two unit tangent vectors of a contact respectively, where $\boldsymbol{n}_i = \boldsymbol{o}_i \times \boldsymbol{t}_i, i = 1, 2, \dots, m$. Assume that each contact is a soft finger contact that can exert a pure force with three components f_{i1}, f_{i2}, f_{i3} along $\boldsymbol{n}_i, \boldsymbol{o}_i, \boldsymbol{t}_i$ and a spin moment f_{i4} about $\boldsymbol{n}_i$ to the object. Then, a contact force can be expressed in the local coordinate frame formed by $\boldsymbol{n}_i$, $\boldsymbol{o}_i$, $\boldsymbol{t}_i$ as $\boldsymbol{f}_i = [f_{i1} \;\; f_{i2} \;\; f_{i3} \;\; f_{i4}]^T$. A grasp is said to be feasible if $\boldsymbol{f}_i$ is in the friction cone F_i, which

The authors are with Disney Research Pittsburgh, PA 15213, USA {yu.zheng, kyamane}@disneyresearch.com

is given by [15]

$$F_i \triangleq \left\{ \boldsymbol{f}_i \in \mathbb{R}^4 \mid f_{i1} \geq 0, \sqrt{\frac{f_{i2}^2 + f_{i3}^2}{\mu_i^2} + \frac{f_{i4}^2}{\mu_{si}^2}} \leq f_{i1} \right\} \quad (1)$$

where μ_i and μ_{si} are the tangential and torsional friction coefficients.

The grasp can resist an external wrench $\boldsymbol{w}$ applied to the object if there exist contact forces $\boldsymbol{f}_i \in F_i$ that satisfy

$$\sum_{i=1}^{m} \boldsymbol{G}_i \boldsymbol{f}_i = \boldsymbol{G}\boldsymbol{f} = -\boldsymbol{w} \quad (2)$$

where $\boldsymbol{G}_i = \begin{bmatrix} \boldsymbol{n}_i & \boldsymbol{o}_i & \boldsymbol{t}_i & \boldsymbol{0} \\ \boldsymbol{p}_i \times \boldsymbol{n}_i & \boldsymbol{p}_i \times \boldsymbol{o}_i & \boldsymbol{p}_i \times \boldsymbol{t}_i & \boldsymbol{n}_i \end{bmatrix} \in \mathbb{R}^{6\times 4}$ is the contact mapping, $\boldsymbol{G} = [\boldsymbol{G}_1 \ \boldsymbol{G}_2 \ \cdots \ \boldsymbol{G}_m] \in \mathbb{R}^{6\times 4m}$ is the grasp matrix, and $\boldsymbol{f} = \begin{bmatrix} \boldsymbol{f}_1^T & \boldsymbol{f}_2^T & \cdots & \boldsymbol{f}_m^T \end{bmatrix}^T \in \mathbb{R}^{4m}$ is the total contact force. A grasp usually needs to have the force closure property, which implies that the grasp can resist any external wrench applied to the object in the 6-D wrench space $\mathbb{R}^6$ [15]. Hereinafter, we only consider force-closure grasps.

Force closure is a basic requirement for a grasp, but does not tell how efficient the grasp is because it may require large contact forces to resist a small external wrench. A more reasonable grasp force efficiency (GFE) measure would be the minimum of the largest wrenches that the grasp can resist with unit total contact force over certain wrench directions of interest [2], [7], [8].

To mathematically formulate the GFE measure, we first define the grasp wrench set (GWS) W, which represents the set of wrenches that a grasp can resist with unit total contact force [8]:

$$W \triangleq \{\boldsymbol{w} = \boldsymbol{G}\boldsymbol{f} \mid \|\boldsymbol{f}\| = 1, \ \boldsymbol{f}_i \in F_i \text{ for } \forall\, i\} \quad (3)$$

where the magnitude $\|\boldsymbol{f}\|$ of $\boldsymbol{f}$ is often defined as the sum or maximum of normal contact forces, i.e.,

$$\|\boldsymbol{f}\|_{L_1} \triangleq \sum_{i=1}^{m} f_{i1} \quad \text{or} \quad \|\boldsymbol{f}\|_{L_\infty} \triangleq \max_{i=1,2,\ldots,m} f_{i1}. \quad (4)$$

Corresponding to different definitions of $\|\boldsymbol{f}\|$ in (4), the GWS W defined by (3) can be rewritten as the convex hull of the union or the Minkowski sum of primitive contact wrench sets W_i, $i = 1, 2, \ldots, m$,

$$W_{L_1} = \mathrm{CH}\left(\bigcup_{i=1}^{m} W_i\right) \quad \text{or} \quad W_{L_\infty} = \mathrm{CH}\left(\bigoplus_{i=1}^{m} W_i\right) \quad (5)$$

where $\mathrm{CH}(\cdot)$ denotes the convex hull of a set and a primitive contact wrench set W_i is the image of a primitive contact force set U_i through the contact mapping $\boldsymbol{G}_i$, i.e.,

$$W_i \triangleq \boldsymbol{G}_i\left(U_i\right) \quad (6)$$

where U_i consists of feasible contact forces with unit normal force component, i.e.,

$$U_i \triangleq \{\boldsymbol{f}_i \in F_i \mid f_{i1} = 1\}. \quad (7)$$

For a force-closure grasp, W contains the origin of $\mathbb{R}^6$ in its interior. The GFE measure can be expressed as the radius of the largest ball contained in W [7] or the minimum distance from the origin to the boundary of W [8]. More generally, the GFE measure can be written as the penetration distance $d_Q(W)$ between the origin of $\mathbb{R}^6$ and W with respect to a set Q [2], which is defined as

$$d_Q(W) \triangleq \max_{\lambda Q \subset W, \lambda \geq 0} \lambda. \quad (8)$$

In other words, $d_Q(W)$ is the maximum scale factor of Q such that the scaled Q is still contained in W. The set Q consists of the wrench directions of interest. In most previous work on GFE evaluation, Q is taken as the unit origin-centered ball [3], [6], [7], [10], [11], i.e., every wrench direction has equal weight. One can also take Q as an ellipsoid to weigh particular wrench directions [8] or a convex polytope to define a task-specific wrench set [2], [4].

In previous work, the contact force magnitude is usually defined by the first equation of (4) so that W can be easily obtained by taking the union of W_i as in the first equation of (5). The other definition of $\|\boldsymbol{f}\|$ is less popular because W is the Minkowski sum of W_i and much more complex, and therefore computing $d_Q(W)$ is much more difficult. By using our algorithm presented in Section IV, in contrast, $d_Q(W)$ can be computed efficiently even for complex W. In addition, the contact force optimization problem [12], [13] is just a special case where Q is a line segment with one endpoint at the origin and the other at the wrench to be resisted.

III. Active Force Efficiency of a Grasp

The conventional GFE measure $d_Q(W)$ used to evaluate and plan grasps [2]–[6], [16] only considers contact positions on the object. Intuitively, however, the grasp quality should change depending on whether each finger has enough active joints or what configuration the robot hand has. Now we take into account the hand structure and configuration in the GFE evaluation. Note that we only consider robot hands consisting of rigid links in this paper, although the compliance of a robot hand may also affect the GFE.

We assume that each finger makes only one contact with the object at the fingertip. The joint torque $\boldsymbol{\tau}_i$ and the contact force $\boldsymbol{f}_i$ at the i-th finger have the relationship

$$\boldsymbol{\tau}_i = \boldsymbol{J}_i^T \boldsymbol{f}_i \quad (9)$$

where $\boldsymbol{J}_i \in \mathbb{R}^{4\times q_i}$ is the Jacobian matrix, $\boldsymbol{\tau}_i \in \mathbb{R}^{q_i}$ is the vector of joint torques, and q_i is the number of degrees of freedom of a finger. Then the pseudo-inverse of $\boldsymbol{J}_i^T$, $\boldsymbol{J}_i^{+T} \in \mathbb{R}^{4\times q_i}$, spans the active contact force space. If we define U_i^a as the intersection of the primitive contact force set U_i and the range of $\boldsymbol{J}_i^{+T}$, we can represent a contact force that can be actively generated by joint torques and satisfies the friction constraint (1) as a nonnegative linear combination of points in U_i^a.

Let r_i be the rank of $\boldsymbol{J}_i^{+T}$. If $r_i = 4$, then the 4-D contact force $\boldsymbol{f}_i$ can be fully generated by joint torques and $U_i^a = U_i$. If $r_i < 4$, then not all contact forces can be actively generated and we calculate U_i^a as follows. Let $\boldsymbol{A}_i \in \mathbb{R}^{4\times r_i}$ be a matrix whose columns constitute a basis for the range of $\boldsymbol{J}_i^{+T}$. Then, an active contact force $\boldsymbol{f}_i^a$ can be written as

$$\boldsymbol{f}_i^a = \boldsymbol{A}_i \boldsymbol{c}_i \quad (10)$$

where $\boldsymbol{c}_i \in \mathbb{R}^{r_i}$. We partition $\boldsymbol{A}_i$ in rows as $\begin{bmatrix} \boldsymbol{A}_{i1} \\ \boldsymbol{A}_{i2} \end{bmatrix}$ such that $f_{i1}^a = \boldsymbol{A}_{i1}\boldsymbol{c}_i$ and $[f_{i2}^a \;\; f_{i3}^a \;\; f_{i4}^a]^T = \boldsymbol{A}_{i2}\boldsymbol{c}_i$, where $\boldsymbol{A}_{i1} \in \mathbb{R}^{1\times r_i}$ and $\boldsymbol{A}_{i2} \in \mathbb{R}^{3\times r_i}$. From (1), (7), and (10), $\boldsymbol{f}_i^a \in U_i$ if and only if the following conditions are satisfied

$$\boldsymbol{A}_{i1}\boldsymbol{c}_i = 1 \tag{11a}$$

$$\boldsymbol{c}_i^T \boldsymbol{A}_{i2}^T \boldsymbol{D}_i \boldsymbol{A}_{i2} \boldsymbol{c}_i \leq 1 \tag{11b}$$

where $\boldsymbol{D}_i = \mathrm{diag}\left\{1/\mu_i^2, 1/\mu_i^2, 1/\mu_{si}^2\right\}$. From (11) we derive a more explicit formulation of U_i^a as below.

1) $r_i = 1$: Equation (11a) gives $c_i = 1/A_{i1}$. If c_i does not satisfy (11b), then there is no active force within the friction cone (1) and $U_i^a = \emptyset$; otherwise we obtain $\boldsymbol{f}_{i0} = \boldsymbol{A}_i/A_{i1}$ and $U_i^a = \{\boldsymbol{f}_{i0}\}$ by substituting c_i into (10).

2) $1 < r_i < 4$: Equation (11a) gives

$$\boldsymbol{c}_i = \boldsymbol{A}_{i1}^+ + \boldsymbol{N}_i \boldsymbol{\lambda} \tag{12}$$

where $\boldsymbol{A}_{i1}^+ \in \mathbb{R}^{r_i}$ is the pseudo-inverse of $\boldsymbol{A}_{i1}$, $\boldsymbol{N}_i \in \mathbb{R}^{r_i\times(r_i-1)}$ spans the null space of $\boldsymbol{A}_{i1}$, and $\boldsymbol{\lambda} \in \mathbb{R}^{r_i-1}$. Substituting (12) into (11b) yields

$$\boldsymbol{\lambda}^T \boldsymbol{Q} \boldsymbol{\lambda} + 2\boldsymbol{b}^T\boldsymbol{\lambda} + c \leq 0 \tag{13}$$

where $\boldsymbol{Q} = \boldsymbol{N}_i^T \boldsymbol{A}_{i2}^T \boldsymbol{D}_i \boldsymbol{A}_{i2} \boldsymbol{N}_i$, $\boldsymbol{b} = \boldsymbol{N}_i^T \boldsymbol{A}_{i2}^T \boldsymbol{D}_i \boldsymbol{A}_{i2} \boldsymbol{A}_{i1}^+$, and $c = \boldsymbol{A}_{i1}^{+T} \boldsymbol{A}_{i2}^T \boldsymbol{D}_i \boldsymbol{A}_{i2} \boldsymbol{A}_{i1}^+ - 1$. Matrix $\boldsymbol{Q}$ is positive definite and can be decomposed as $\boldsymbol{Q} = \boldsymbol{U}^T\boldsymbol{U}$, where $\boldsymbol{U}$ is an upper triangular matrix with positive diagonal entries. By a few matrix manipulations, we can further reduce (13) to

$$\boldsymbol{x}^T\boldsymbol{x} \leq \Delta \tag{14}$$

where $\boldsymbol{x} = \boldsymbol{U}\boldsymbol{\lambda} + \boldsymbol{U}^{-T}\boldsymbol{b}$ and $\Delta = \boldsymbol{b}^T\boldsymbol{Q}^{-1}\boldsymbol{b} - c$. Substituting $\boldsymbol{\lambda} = \boldsymbol{U}^{-1}\boldsymbol{x} - \boldsymbol{Q}^{-1}\boldsymbol{b}$ into (12) and substituting the resulting $\boldsymbol{c}_i$ into (10), we obtain

$$\boldsymbol{f}_i^a = \boldsymbol{f}_{i0} + \boldsymbol{P}_i\boldsymbol{x} \tag{15}$$

where $\boldsymbol{f}_{i0} = \boldsymbol{A}_i(\boldsymbol{A}_{i1}^+ - \boldsymbol{N}_i\boldsymbol{Q}^{-1}\boldsymbol{b})$ and $\boldsymbol{P}_i = \boldsymbol{A}_i\boldsymbol{N}_i\boldsymbol{U}^{-1}$. Depending on the sign of Δ, we have

- $\Delta < 0$: No active contact force satisfies the friction constraint (1) and $U_i^a = \emptyset$.
- $\Delta = 0$: U_i^a consists only of $\boldsymbol{f}_{i0}$ in (15), i.e., $U_i^a = \{\boldsymbol{f}_{i0}\}$, and spans a 1-D subspace of the 4-D contact force space at contact i.
- $\Delta > 0$: U_i^a is expressed by (14) and (15) and it spans an r_i-D subspace of the 4-D contact force space.

Taking linearly independent elements of U_i^a, we construct a matrix $\boldsymbol{B}_i$ that gives a basis for the minimal space containing all active feasible contact forces at contact i. Then, the minimal wrench space containing the wrenches that can be generated by active feasible contact forces from all contacts is spanned by $\boldsymbol{W} = [\boldsymbol{G}_1\boldsymbol{B}_1 \;\; \boldsymbol{G}_2\boldsymbol{B}_2 \;\; \cdots \;\; \boldsymbol{G}_m\boldsymbol{B}_m]$, and we can compute its orthonormal basis $\boldsymbol{R}$ by the singular value decomposition of $\boldsymbol{W}$.

Similarly to (6), we define $W_i^a \triangleq \boldsymbol{G}_i\left(U_i^a\right)$ as an active primitive contact wrench set, which consists of primitive contact wrenches that can be generated by joint torques through contact i. Then, the active GWS, denoted by W^a, can be written as (5) with W_i^a replacing W_i, and it comprises all wrenches that can be generated by unit active feasible contact forces on the object. The range of $\boldsymbol{R}$ is the minimal subspace of $\mathbb{R}^6$ that contains W^a.

In summary, we first determine the dimension of the minimal space containing W^a, which is equal to the rank of $\boldsymbol{R}$. Then, we check if the origin of the minimal space is contained in the interior of W^a, which implies that all wrenches in the minimal space can be generated only by joint torques. Furthermore, we can evaluate the active GFE by $d_Q(W^a)$, which can also be formulated as (8) with W^a replacing W and computed by our algorithm proposed in Section IV, where Q is a compact convex set containing the origin in the minimal space.

IV. Generalized Penetration Distance Algorithm

A. Definition of Generalized Penetration Distance

From the above arguments, both the original GFE measure [2], [8] and the active GFE measure can be expressed as the penetration distance $d_Q(A)$ between the origin of space $\mathbb{R}^n$ and a compact convex set A with respect to another compact convex set Q:

$$d_Q(A) \triangleq \max_{\lambda Q \subset A, \lambda \geq 0} \lambda \tag{16}$$

where A has a nonempty interior that contains the origin, while Q contains the origin and can be of any dimension. As illustrated in Fig. 1a, $d_Q(A)$ is the maximum scale factor λ such that λQ is contained in A. For the GFE measures here, A corresponds to W or W^a defined in the previous two sections while set Q determines the distance metric. If Q is the unit origin-centered ball, $d_Q(A)$ is simply the traditional penetration distance in the 2-norm sense [17]. The definition also includes 1-norm or infinity-norm distances as special cases of Q being corresponding polytopes.

We can also relax the original definition of $d_Q(A)$ in [2] by allowing Q of a dimension smaller than that of the space or with the origin on its boundary rather than in its interior. In the extreme case where Q is a line segment starting from the origin, the problem degenerates to the ray-shooting problem to compute the farthest intersection point of A with the ray along the line segment [12]–[14]. Therefore, $d_Q(A)$ defined by (16) gives a generalized penetration distance and unifies many quantities related to grasp force.

So far, however, there is no algorithm to compute $d_Q(A)$ for compact convex sets A and Q with exact parametric representation. Zhu et al. [2], [16] computed $d_Q(A)$ by solving linear programs when both A and Q are polytope approximations. In this section, we present an algorithm for the general case, so that the GFE measures can be calculated without linear approximation.

B. Other Definitions and Notations

In the following discussion, we will often use the support function h_A and the support mapping $\boldsymbol{s}_A$ of a set A [18]:

$$h_A(\boldsymbol{u}) \triangleq \max_{\boldsymbol{a}\in A} \boldsymbol{u}^T\boldsymbol{a}, \quad \boldsymbol{s}_A(\boldsymbol{u}) \triangleq \arg\max_{\boldsymbol{a}\in A} \boldsymbol{u}^T\boldsymbol{a} \tag{17}$$

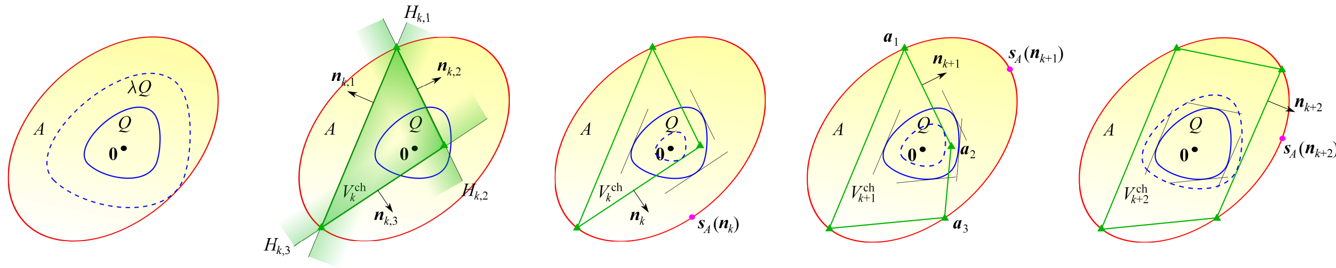

(a) (b) (c) (d) (e)

Fig. 1. Illustration of the generalized penetration distance and its computation in 2-D space. (a) The generalized penetration distance $d_Q(A)$ defined as the maximal scale factor λ of a compact convex set Q such that λQ is contained in a compact convex set A. (b) Polytope $V_k^{\rm ch}$ as the intersection of a set of half-spaces $H_{k,j}^-$, i.e., $V_k^{\rm ch} = \bigcap_{j=1,2,\ldots,N_k} H_{k,j}^-$, where $H_{k,j}^-$ is the shadowed side of the hyperplane $H_{k,j}$ that contains a facet of $V_k^{\rm ch}$. (c)–(e) Polytope $V_k^{\rm ch}$ growing through the iteration process $V_{k+1} = V_k \cup \{\boldsymbol{s}_A(\boldsymbol{n}_k)\}$ such that $d_k = d_Q(V_k^{\rm ch})$ increases and eventually converges to $d_Q(A)$. The dashed line outlines the set d_kQ, which is contained in $V_k^{\rm ch}$. $\boldsymbol{s}_A(\boldsymbol{n}_k)$ is the farthest point in A from the origin along the normal $\boldsymbol{n}_k$ of the facet of $V_k^{\rm ch}$ that strictly bounds d_kQ. In (d), two of the facets of $V_{k+1}^{\rm ch}$ separate $\boldsymbol{s}_A(\boldsymbol{n}_{k+1})$ from $d_{k+1}Q$ and therefore will be the eliminated facets (Proposition 3). Then, as shown in (e), the facet formed by $\boldsymbol{s}_A(\boldsymbol{n}_{k+1})$ and the point $\boldsymbol{a}_2$ shared by the eliminated facets is contained in the interior of $V_{k+2}^{\rm ch}$, while the facets formed by $\boldsymbol{s}_A(\boldsymbol{n}_{k+1})$ and other points $\boldsymbol{a}_1$ and $\boldsymbol{a}_3$ are facets of $V_{k+2}^{\rm ch}$.

where $\boldsymbol{u}$ is an arbitrary vector in $\mathbb{R}^n$. The support function h_A is a scalar-valued function, while the support mapping $\boldsymbol{s}_A$ returns a point in A such that $h_A(\boldsymbol{u}) = \boldsymbol{u}^T\boldsymbol{s}_A(\boldsymbol{u})$. Using the support function and mapping of A and Q, we can first derive the following result. Due to the page limit, we omit the proof of all propositions herein and will include it in a complete version of this paper.

Proposition 1: $d_Q(A) = \min_{\boldsymbol{u}^T\boldsymbol{u}=1} \frac{h_A(\boldsymbol{u})}{h_Q(\boldsymbol{u})}$.

Let V_k be a finite subset of A such that its convex hull $V_k^{\rm ch}$ is an n-dimensional polytope in A and contains the origin of $\mathbb{R}^n$, as depicted in Fig. 1b. The members of V_k do not have to be on the boundary of A. Assume that $V_k^{\rm ch}$ has N_k facets and each facet has affinely-independent n vertices. Let $V_{k,j}$ ($j = 1, 2, \ldots, N_k$) be the set of vertices of facet j, $H_{k,j}$ the hyperplane containing facet j, and $\boldsymbol{n}_{k,j}$ the common normal of $H_{k,j}$ and facet j. We choose the length of $\boldsymbol{n}_{k,j}$ such that $H_{k,j}$ is expressed as

$$H_{k,j} \triangleq \left\{\boldsymbol{a} \in \mathbb{R}^n \mid \boldsymbol{n}_{k,j}^T\boldsymbol{a} = \delta_{k,j}\right\} \tag{18}$$

where $\delta_{k,j} = 1$ if $H_{k,j}$ does not pass through the origin (i.e., $V_{k,j}$ is linearly independent) and $\delta_{k,j} = 0$ otherwise (i.e., $V_{k,j}$ is linearly dependent). Each hyperplane $H_{k,j}$ divides the whole space $\mathbb{R}^n$ into two closed half-spaces

$$H_{k,j}^- \triangleq \left\{\boldsymbol{a} \in \mathbb{R}^n \mid \boldsymbol{n}_{k,j}^T\boldsymbol{a} \le \delta_{k,j}\right\} \tag{19a}$$

$$H_{k,j}^+ \triangleq \left\{\boldsymbol{a} \in \mathbb{R}^n \mid \boldsymbol{n}_{k,j}^T\boldsymbol{a} \ge \delta_{k,j}\right\}. \tag{19b}$$

We set $\boldsymbol{n}_{k,j}$ so that it points the opposite side of $H_{k,j}$ to $V_k^{\rm ch}$ and therefore $V_k^{\rm ch}$ lies in $H_{k,j}^-$ (see Fig. 1b). Then, the origin of $\mathbb{R}^n$, which is contained in $V_k^{\rm ch}$, also lies in $H_{k,j}^-$. Noting that Q contains the origin, we define $d_{k,j}$ as

$$d_{k,j} \triangleq \max_{\lambda Q \subset H_{k,j}^-, \lambda \ge 0} \lambda. \tag{20}$$

The value $d_{k,j}$ can be regarded as the distance of $H_{k,j}$ from the origin with respect to Q. Let d_k be the minimum of $d_{k,j}$ for $j = 1, 2, \ldots, N_k$, i.e.,

$$d_k \triangleq \min_{j=1,2,\ldots,N_k} d_{k,j} = \min_{j=1,2,\ldots,N_k} \max_{\lambda Q \subset H_{k,j}^-, \lambda \ge 0} \lambda. \tag{21}$$

Also, let $j_k \triangleq \arg\min_{j=1,2,\ldots,N_k} d_{k,j}$ and $\boldsymbol{n}_k \triangleq \boldsymbol{n}_{k,j_k}$.

The normal $\boldsymbol{n}_{k,j}$ of $H_{k,j}$ can be calculated as follows. If $V_{k,j}$ is linearly independent, then $\boldsymbol{n}_{k,j}$ is the solution to the linear equation

$$\boldsymbol{V}_{k,j}^T\boldsymbol{n}_{k,j} = \mathbf{1} \tag{22}$$

where $\boldsymbol{V}_{k,j} \in \mathbb{R}^{n\times n}$ is the matrix whose columns are the points in $V_{k,j}$ and $\mathbf{1} = [1 \quad 1 \quad \cdots \quad 1]^T \in \mathbb{R}^n$. Furthermore, we can derive

$$d_{k,j} = \frac{h_{V_{k,j}}(\boldsymbol{n}_{k,j})}{h_Q(\boldsymbol{n}_{k,j})} = \frac{1}{h_Q(\boldsymbol{n}_{k,j})}. \tag{23}$$

If $V_{k,j}$ is linearly dependent, then $\boldsymbol{n}_{k,j}$ is a nonzero vector in the null space of $\boldsymbol{V}_{k,j}^T$, having negative inner product with any point in $V_k \setminus V_{k,j}$, such that $V_k^{\rm ch} \subset H_{k,j}^-$. If $h_Q(\boldsymbol{n}_{k,j}) \ne 0$, then $d_{k,j} = 0$; otherwise, $d_{k,j} = +\infty$. From these arguments, we can write $d_{k,j}$ as

$$d_{k,j} = \begin{cases} \delta_{k,j}/h_Q(\boldsymbol{n}_{k,j}) & \text{if } h_Q(\boldsymbol{n}_{k,j}) \ne 0 \\ +\infty & \text{if } h_Q(\boldsymbol{n}_{k,j}) = 0. \end{cases} \tag{24}$$

From the above definitions, the convexity of $V_k^{\rm ch}$, and the fact that $V_k^{\rm ch} = \bigcap_{j=1,2,\ldots,N_k} H_{k,j}^-$ [18] as depicted in Fig. 1b, we can deduce the following results.

Proposition 2: The following statements are true:

1) Hyperplane $H_{k,j}$ supports $d_{k,j}Q$ at $d_{k,j}\boldsymbol{s}_Q(\boldsymbol{n}_{k,j})$ and $d_{k,j}Q$ is in $H_{k,j}^-$;
2) d_kQ is contained in $V_k^{\rm ch}$;
3) $d_k = \max_{\lambda Q \subset V_k^{\rm ch}, \lambda \ge 0} \lambda = d_Q(V_k^{\rm ch})$.

Fig. 1c gives an illustration of Proposition 2 3), where the dashed line represents d_kQ.

C. Iteration Process

The algorithm for computing the generalized penetration distance iteratively expands polytope $V_k^{\rm ch}$ in A such that $d_k = d_Q(V_k^{\rm ch})$ converges to $d_Q(A)$. This subsection describes the iteration process.

Figure 1c implies that d_kQ, contained in $V_k^{\rm ch}$, is strictly bounded by facet j_k of $V_k^{\rm ch}$. Along the normal $\boldsymbol{n}_k$ of facet

j_k, we obtain the support mapping $\boldsymbol{s}_A(\boldsymbol{n}_k)$ of A, which is located in the half-space H^+_{k,j_k} if $h_A(\boldsymbol{n}_k) > \delta_{k,j_k}$. Then, taking $V_{k+1} = V_k \cup \{\boldsymbol{s}_A(\boldsymbol{n}_k)\}$, we can obtain V^{ch}_{k+1} that contains facet j_k of V^{ch}_k in its interior and provides a bigger polytope in A than V^{ch}_k, as depicted in Fig. 1d. If there is only one facet that strictly bounds d_kQ, then we have $d_{k+1} = d_Q(V^{\text{ch}}_{k+1}) > d_k$. Even if there are multiple facets strictly bounding d_kQ, with a finite number of iterations we can still obtain a polytope that contains all those facets in its interior and get d_k increased, since the number of such facets is finite. By this iteration, therefore, $d_k = d_Q(V^{\text{ch}}_k)$ increases as the polytope V^{ch}_k grows. On the other hand, since V^{ch}_k is always contained in A, d_k has the upper bound of $d_Q(A)$. Thus, by the monotone-convergence principle [19], it is guaranteed that d_k converges. As the iteration proceeds, condition $h_A(\boldsymbol{n}_k) - \delta_{k,j_k} \le \epsilon h_Q(\boldsymbol{n}_k)$, where $\epsilon \ge 0$ is the termination tolerance, will eventually be satisfied, and it implies that facet j_k of V^{ch}_k that strictly bounds d_kQ is close to the boundary of A. Furthermore, since $d_k = \delta_{k,j_k}/h_Q(\boldsymbol{n}_k)$ from (24) and $d_Q(A) \le h_A(\boldsymbol{n}_k)/h_Q(\boldsymbol{n}_k)$ from Proposition 1, we can derive $0 \le d_Q(A) - d_k \le \epsilon$ if $h_A(\boldsymbol{n}_k) - \delta_{k,j_k} \le \epsilon h_Q(\boldsymbol{n}_k)$. Hence, the accuracy of the result from the iteration can be easily specified by setting an appropriate ϵ.

As shown in Figs. 1c–1e, V^{ch}_{k+1} shares many common facets with V^{ch}_k. With the help of this property, we can quickly compute V^{ch}_{k+1} from V^{ch}_k as below. First, the following proposition gives a necessary and sufficient condition for a facet of V^{ch}_k to be a facet of V^{ch}_{k+1}:

Proposition 3: If $\boldsymbol{n}^T_{k,j}\boldsymbol{s}_A(\boldsymbol{n}_k) > \delta_{k,j}$, then $\boldsymbol{s}_A(\boldsymbol{n}_k) \in H^+_{k,j}$, and facet j of V^{ch}_k is contained in the interior of V^{ch}_{k+1} and not a facet of V^{ch}_{k+1}; otherwise it is a facet of V^{ch}_{k+1}.

We call a facet of V^{ch}_k for which $\boldsymbol{n}^T_{k,j}\boldsymbol{s}_A(\boldsymbol{n}_k) > \delta_{k,j}$ an eliminated facet. There could be multiple eliminated facets as shown in Figs. 1d and 1e. Note that each facet of V^{ch}_k is an $(n-1)$-dimensional simplex having n facets of dimension $n-2$. Let $V_{k,j,l}$ $(l = 1, 2, \dots, n)$ be a subset of $n-1$ elements of $V_{k,j}$. Then, $V^{\text{ch}}_{k,j,l}$ is a facet of facet j of V^{ch}_k. The following proposition indicates how to find new facets of V^{ch}_{k+1} other than those inherited from V^{ch}_k:

Proposition 4: Assume that facet j of V^{ch}_k, namely $V^{\text{ch}}_{k,j}$, is an eliminated facet and $V^{\text{ch}}_{k,j,l}$ is a facet of facet j. If $V^{\text{ch}}_{k,j,l}$ is not a facet of an eliminated facet of V^{ch}_k other than facet j, then the convex hull of $V_{k,j,l} \cup \{\boldsymbol{s}_A(\boldsymbol{n}_k)\}$ is a new facet of V^{ch}_{k+1}; otherwise, it is contained in the interior of V^{ch}_{k+1} and therefore not a facet of V^{ch}_{k+1}.

Clearly the convex hull of $\boldsymbol{s}_A(\boldsymbol{n}_k)$ with a common facet of two eliminated facets is in the interior of the convex hull of $\boldsymbol{s}_A(\boldsymbol{n}_k)$ with the two facets and is in the interior of V^{ch}_{k+1}, as illustrated in Fig. 1d. If $V^{\text{ch}}_{k,j,l}$ is a facet of only one eliminated facet, then the hyperplane containing the convex hull of $V_{k,j,l} \cup \{\boldsymbol{s}_A(\boldsymbol{n}_k)\}$ bounds V_{k+1} to one side, which implies the convex hull of $V_{k,j,l} \cup \{\boldsymbol{s}_A(\boldsymbol{n}_k)\}$ is a facet of V^{ch}_{k+1}. By verifying Proposition 4 for the facets of every eliminated facet of V^{ch}_k, we can find all new facets of V^{ch}_{k+1}, for which $\boldsymbol{n}_{k+1,j}$ and $d_{k+1,j}$ can be easily calculated as discussed in Section IV-B.

Algorithm 1 Algorithm for the Generalized Penetration Distance

Input: compact convex sets A and Q
Output: the generalized penetration distance $d_Q(A)$
compute an initial set V_0
compute $V_{0,j}$, $\boldsymbol{n}_{0,j}$, and $d_{0,j}$ for $j = 1, 2, \dots, N_0$
$j_0 \leftarrow \arg\min_{j=1,2,\dots,N_0} d_{0,j}$, $d_0 \leftarrow d_{0,j_0}$, $\boldsymbol{n}_0 \leftarrow \boldsymbol{n}_{0,j_0}$
$k \leftarrow 0$
while $h_A(\boldsymbol{n}_k) - \delta_{k,j_k} > \epsilon h_Q(\boldsymbol{n}_k)$ **do**
  $V_{k+1} \leftarrow V_k \cup \{\boldsymbol{s}_A(\boldsymbol{n}_k)\}$, $k \leftarrow k+1$
  update $V_{k,j}$, $\boldsymbol{n}_{k,j}$, and $d_{k,j}$ for $j = 1, 2, \dots, N_k$
  $j_k \leftarrow \arg\min_{j=1,2,\dots,N_k} d_{k,j}$, $d_k \leftarrow d_{k,j_k}$, $\boldsymbol{n}_k \leftarrow \boldsymbol{n}_{k,j_k}$
end while
return d_k

It turns out that the increase in the number of facets of V^{ch}_k by every iteration is bounded above by the space dimension, which is a constant. Thus, the number of facets of V^{ch}_k is linear in the number of conducted iterations. Moreover, the computation cost for every iteration is proportional to the number of facets of V^{ch}_k, as we need to seek the eliminated facets of V^{ch}_k, whereas the rest of computation is of constant complexity. Therefore, the total complexity of our algorithm is quadratic to the number of iterations until stop.

D. Initialization of the Algorithm

Now the only problem is how to find a finite subset V_0 of A such that its convex hull V^{ch}_0 contains the origin and gives an initial n-dimensional polytope for the iteration. To do this, we employ the GJK algorithm [20] to compute the minimum Euclidean distance between the origin and the set A. Since A contains the origin, the GJK algorithm yields p affinely independent points in A, denoted by $\boldsymbol{a}_1, \boldsymbol{a}_2, \dots, \boldsymbol{a}_p$, whose convex hull contains the origin, where $p \le n+1$. If $p = n+1$, then we simply set $V_0 = \{\boldsymbol{a}_1, \boldsymbol{a}_2, \dots, \boldsymbol{a}_p\}$. If $p < n+1$, we can add another point $\boldsymbol{a}_{p+1} = \boldsymbol{s}_A(\boldsymbol{u})$ that can be proved to be affinely independent with $\boldsymbol{a}_0, \boldsymbol{a}_1, \dots, \boldsymbol{a}_p$, where $\boldsymbol{u}$ is any nonzero vector in $\mathbb{R}^n$ orthogonal to $\boldsymbol{a}_1, \boldsymbol{a}_2, \dots, \boldsymbol{a}_p$. We can repeat this process until we obtain $n+1$ affinely independent points to form V_0. The polytope V^{ch}_0 constructed in this way is an n-dimensional simplex, so it is easy to determine its facets and the values $\boldsymbol{n}_{0,j}$ and $d_{0,j}$ for each facet.

V. Numerical Examples

We verify the usefulness and performance of our algorithm using a four-finger robot hand grasping a block as shown in Fig. 2. Each finger has four joints, of which joints 1–3 are active and joint 4 is coupled to joint 3 at a ratio of 1:1. The proposed algorithm is implemented in MATLAB on a laptop with an Intel Core i7 2.67GHz CPU and 3GB RAM. Our implementation is applicable to any W and Q but is not particularly optimized. The termination tolerance ϵ for the algorithm is set to 10^{-4} and the set W (or W^a) is taken to be the Minkowski sum of W_i (or W^a_i), as defined by the second equation in (6), which is more complex. Unless otherwise indicated, Q is taken to be the unit origin-centered ball in $\mathbb{R}^6$ or the space spanned by $\boldsymbol{R}$. The friction coefficients are $\mu_i = 0.2$ and $\mu_{si} = 0.2$. The algorithm to compute $d_Q(W)$ or $d_Q(W^a)$ (Section IV) requires the computation of the

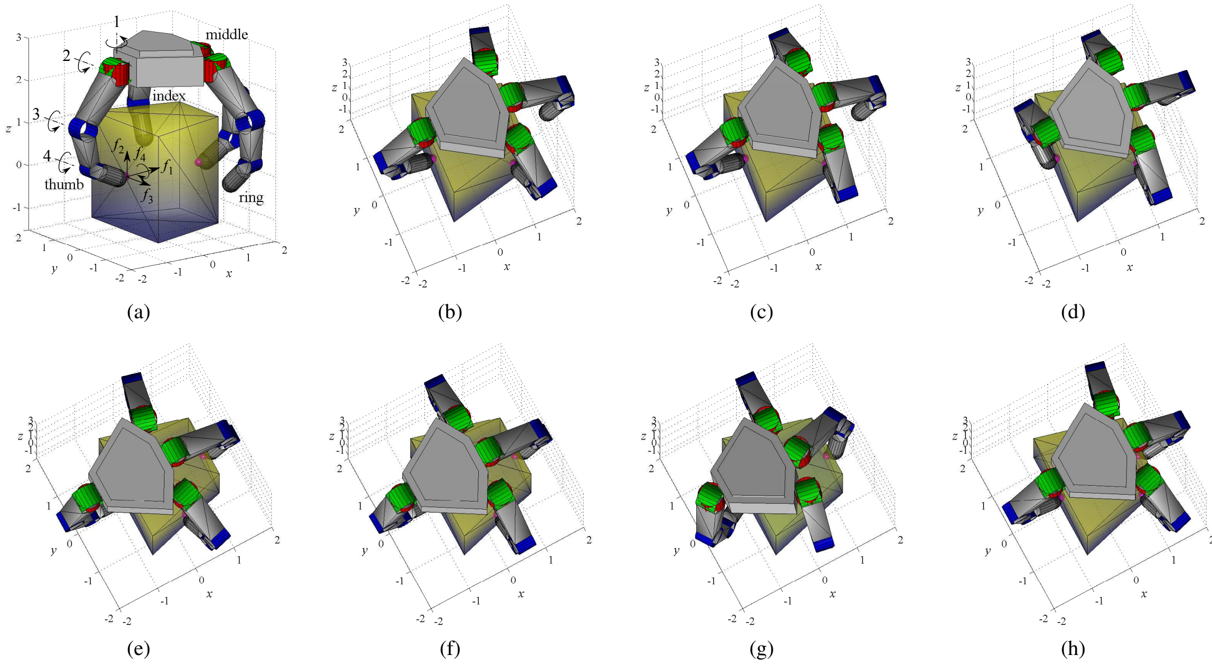

Fig. 2. A block grasped by (a) two fingers, (b)–(d) three fingers, and (e)–(h) four fingers. (a) Joint 1 (drawn in red) is locked. (b) Joint 1 may be locked or activated. The joint axes are parallel to the face. (c),(d) The robot hand has a different position or orientation from (b) but the contact positions are the same and the joint axes are no longer parallel to the face. (e) Joint 1 may be locked or activated and the joint axes are parallel to the face. (f),(g) The robot hand has a different position or orientation from (e) while maintaining the same contact positions and the joint axes are no longer parallel to the face. (h) The joint axes are parallel to the face but two contact positions on the block are different from (e).

support function and mapping of W_i (or W_i^a), for which we employ the closed-form expressions derived in [21], [22].

We test our algorithm in the following situations:

- (a1) The thumb and middle fingers grasp the block at the centroids of two opposite faces as shown in Fig. 2a. Joint 1 (drawn in red) of each finger is locked to constrain the motion in a plane.
- (a2) Same as (a1) but Q is an origin-centered ellipsoid with the semi-major axis of length 2 and semi-minor axes of length 1, instead of the unit ball.
- (a3) Same as (a1) but Q is an origin-centered polytope such that $d_Q(W)$ is the 1-norm distance.
- (a4) Same as (a1) but Q is an origin-centered hypercube such that $d_Q(W)$ is the infinity-norm distance.
- (a5) Same as (a1) but Q is the line segment on the x axis with $x = [-1, 1]$.
- (b1) The thumb, index, and ring fingers grasp the object at the centroids of corresponding faces (Fig. 2b). Joint 1 of each finger is locked. The axes of other joints are parallel to the face which the finger is in contact with.
- (b2) Same as (b1) but joint 1 is not locked.
- (c) Same as (b2) but the hand has been shifted along the x axis while keeping the same contact positions on the block (Fig. 2c). The joint axes of the index and ring fingers are no longer parallel to the faces.
- (d) Same as (b2) but the hand has been rotated about the x-axis while keeping the same contact positions (Fig. 2d). The joint axes of all three fingers are no longer parallel to the faces.
- (e1) All four finger grasp the object at the centroid of each face (Fig. 2e). Joint 1 is locked. The joint axes of other joints are parallel to the face.
- (e2) Same as (e1) but joint 1 is not locked.
- (f) Same as (e2) but the hand has been shifted along the x axis while keeping the same contact positions (Fig. 2f). The joint axes of the index and ring fingers are no longer parallel to the faces.
- (g) Same as (e2) but the hand has been rotated about the x axis while keeping the same contact positions (Fig. 2g). The joint axes of all four joints are not parallel to the faces.
- (h) Same as (e2) but the hand has been shifted along the x axis and the contact positions of the index and ring fingers also change to keep the joint axes parallel to the faces (Fig. 2h).

Table I summarizes the results. Without considering the structure of the robot hand, W spans the whole 6-D wrench space in all the situations. When joint 1 is locked, however, it is clear that not all contact forces can be actively generated by joint torques, which leads to the result that the space spanned by W^a is 3-D or 5-D. In (b)–(d) and (e)–(g), $d_Q(W)$ has the same value for the same contact positions, while $d_Q(W^a)$ changes due to the difference in the hand configuration. Furthermore, since the joint axes of fingers in (b2) and (e2) are parallel to the faces, a wider range of contact forces in the friction cone can be generated by joint torques. As a result, $d_Q(W^a)$ in (b2) and (e2) is larger than that in the other situations. In (h), due to the

TABLE I. RESULTS OF EXAMPLES

Ex	$d_Q(W)$	K	t_{CPU}	Dim	$d_Q(W^a)$	K	t_{CPU}
(a1)	0.2425	437	155.18	3	0.2425	3	0.0028
(a2)	0.2235	359	108.93	3	0.2236	4	0.0040
(a3)	0.3154	96	11.330	3	0.3155	3	0.0039
(a4)	0.1119	82	6.1654	3	0.1513	4	0.0032
(a5)	1.0000	18	0.2989	3	1.0000	2	0.0026
(b1)	0.3399	169	19.997	5	0.1238	4	0.0144
(b2)				6	0.2131	104	9.4171
(c)				6	0.0720	38	1.0430
(d)				6	0.1087	25	0.3657
(e1)	0.5624	186	21.907	5	0.3586	23	0.0966
(e2)				6	0.3693	90	5.8219
(f)				6	0.0395	16	0.2188
(g)				6	0.1536	27	0.5031
(h)	0.4916	243	35.923	6	0.2882	79	3.9711

Dim — Dimension of the space spanned by W^a.
K — Number of iterations of our algorithm.
t_{CPU} — CPU running time of an algorithm (unit: second).

change of contact positions, $d_Q(W^a)$ drops in comparison to (e2). Table I demonstrates that $d_Q(W^a)$ provides a more reasonable measure for rating grasps. Finally, Fig. 3 shows the actual shape of W^a for (a1)–(a5) where W^a is 3-D and can be visualized.

The number of iterations and CPU running time of our algorithm are also shown in Table I, which demonstrates that our algorithm is generally fast enough for practical use. In some cases, however, it takes many iterations to reach the termination tolerance $\epsilon = 10^{-4}$. This is because the origin is deep inside W or W^a and the distances from the origin to its boundary are similar in many different directions due to the symmetric layout of contact positions and/or fingers on the object, particularly in (a), (b2), and (e2). The value of d_k and the square root of the CPU running time versus the iteration of our algorithm in (b2), (e2), and (h) are plotted in Fig. 4, which clearly shows that the time complexity of our algorithm is quadratic to the number of iterations.

VI. CONCLUSIONS AND FUTURE WORK

This paper first presented a new GFE measure that considers the hand structure and configuration. The new measure gives a more reasonable evaluation of grasp quality when the fingers cannot produce contact forces uniformly in all directions due to, for example, the finger pose and joint couplings. It would be a useful tool not only for grasp planning but also for hand mechanism design.

We then developed a new algorithm for computing the generalized penetration distance and applied it to the GFE measure. The algorithm provides a unified way to compute the penetration distance with different metrics, including the standard 2-norm. It also allows the computation of generalized GFE measure where the GWS and its inscribed set can have various definitions and choices.

Future work includes verifying the new GFE measure by more experiments with different robot hands and complex objects, and applying the measure to integrated grasp planning of both contact points and hand configurations. It has been noticed in given numerical examples that the CPU time of our algorithm can be long sometimes, especially for grasps of good quality. Hence, we may need other ways to speed up the algorithm for it to be applicable to online computation. In addition, we would like to explore other applications of the generalized distance computation algorithm such as locomotion and haptics.

REFERENCES

[1] K. B. Shimoga, "Robot grasp synthesis algorithms: a survey," *International Journal of Robotics Research*, vol. 15, no. 3, pp. 230–266, 1996.

[2] X.-Y. Zhu and J. Wang, "Synthesis of force-closure grasps on 3-D objects based on the Q distance," *IEEE Transactions on Robotics and Automation*, vol. 19, no. 4, pp. 669–679, 2003.

[3] A. T. Miller and P. K. Allen, "GraspIt! a versatile simulator for robotic grasping," *IEEE Robotics & Automation Magazine*, vol. 11, no. 4, pp. 110–122, 2004.

[4] T. Watanabe and T. Yoshikawa, "Grasping optimization using a required external force set," *IEEE Transactions on Automation Science and Engineering*, vol. 4, no. 1, pp. 52–66, 2007.

[5] Z. X. Xue, J. M. Zoellner, and R. Dillmann, "Automatic optimal grasp planning based on found contact points," in *Proceedings of the IEEE/ASME International Conference on Advanced Intelligent Mechatronics*, Xi'an, China, July 2008, pp. 1053–1058.

[6] M. A. Roa and R. Suárez, "Computation of independent contact regions for grasping 3-D objects," *IEEE Transactions on Robotics*, vol. 25, no. 4, pp. 839–850, 2009.

[7] D. Kirkpatrick, B. Mishra, and C. Yap, "Quantitative steinitzs theorem with applications to multi-fingered grasping," in *Proceedings of the 22th ACM Symposium on Theory of Computing*, New York, NY, 1990, pp. 341–351.

[8] C. Ferrari and J. Canny, "Planning optimal grasps," in *Proceedings of the IEEE International Conference on Mechatronics and Automation*, Nice, France, 1992, pp. 2290–2295.

[9] M. Ceccarelli, *Fundamentals of Mechanics of Robotic Manipulation*. Norwell, MA, USA: Springer, 2004.

[10] A. T. Miller and P. K. Allen, "Examples of 3D grasp quality computation," in *Proceedings of the IEEE International Conference on Robotics and Automation*, Detroit, MI, 1999, pp. 1240–1246.

[11] C. Borst, M. Fischer, and G. Hirzinger, "A fast and robust grasp planner for arbitrary 3D objects," in *Proceedings of the IEEE International Conference on Mechatronics and Automation*, Detroit, Michigan, May 1999, pp. 1890–1896.

[12] Y.-H. Liu, "Qualitative test and force optimization of 3-D frictional form-closure grasps using linear programming," *IEEE Transactions on Robotics and Automation*, vol. 15, no. 1, pp. 163–173, 1999.

[13] Y. Zheng, M. C. Lin, and D. Manocha, "A fast *n*-dimensional ray-shooting algorithm for grasping force optimization," in *Proceedings of the IEEE International Conference on Robotics and Automation*, Anchorage, Alaska, May 2010, pp. 1300–1305.

[14] Y. Zheng and K. Yamane, "Ray-shooting algorithms for robotics," in *Proceedings of the International Workshop on the Algorithmic Foundations of Robotics*, Cambridge, MA, June 2012, in press.

[15] R. M. Murray, Z. X. Li, and S. S. Sastry, *A Mathematical Introduction to Robotic Manipulation*. Boca Raton, FL, USA: CRC Press, 1994.

[16] X.-Y. Zhu, H. Ding, and S. K. Tso, "A pseudodistance function and its applications," *IEEE Transactions on Robotics and Automation*, vol. 20, no. 2, pp. 344–352, 2004.

[17] C. J. Ong and E. G. Gilbert, "Growth distance: New measures for object separation and penetration," *IEEE Transactions on Robotics and Automation*, vol. 12, no. 6, pp. 888–903, 1996.

[18] S. R. Lay, *Convex Sets and their Applications*. New York, NY, USA: John Wiley & Sons, 1982.

[19] W. Rudin, *Principles of Mathematical Analysis*, 3rd ed. New York, NY, USA: McGraw-Hill, 1976.

[20] E. G. Gilbert, D. W. Johnson, and S. S. Keerthi, "A fast procedure for computing the distance between complex objects in three-dimensional space," *IEEE Transactions on Robotics and Automation*, vol. 4, no. 2, pp. 193–203, 1988.

[21] Y. Zheng and C.-M. Chew, "Distance between a point and a convex cone in *n*-dimensional space: computation and applications," *IEEE Transactions on Robotics*, vol. 25, no. 6, pp. 1397–1412, 2009.

[22] Y. Zheng and W.-H. Qian, "Improving grasp quality evaluation," *Robotics and Autonomous Systems*, vol. 57, no. 6-7, pp. 665–673, 2009.

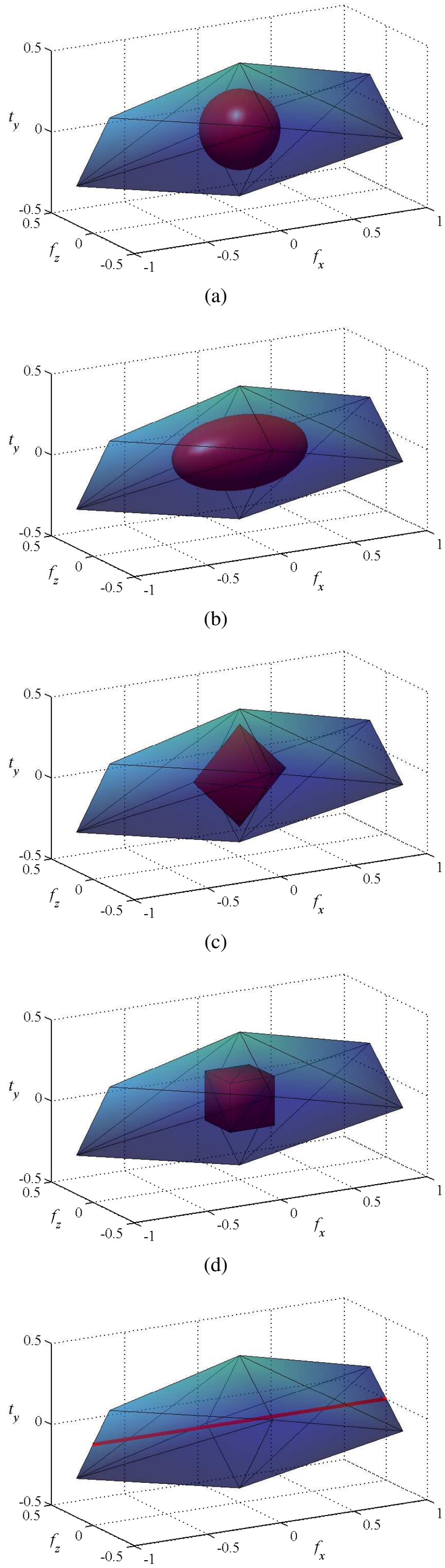

Fig. 3. Active grasp wrench set W^a (in blue color) and its largest inscribed set $d_Q(W^a)Q$ (in red color) shown in the minimal space containing W^a in the case of (a1)–(a5).

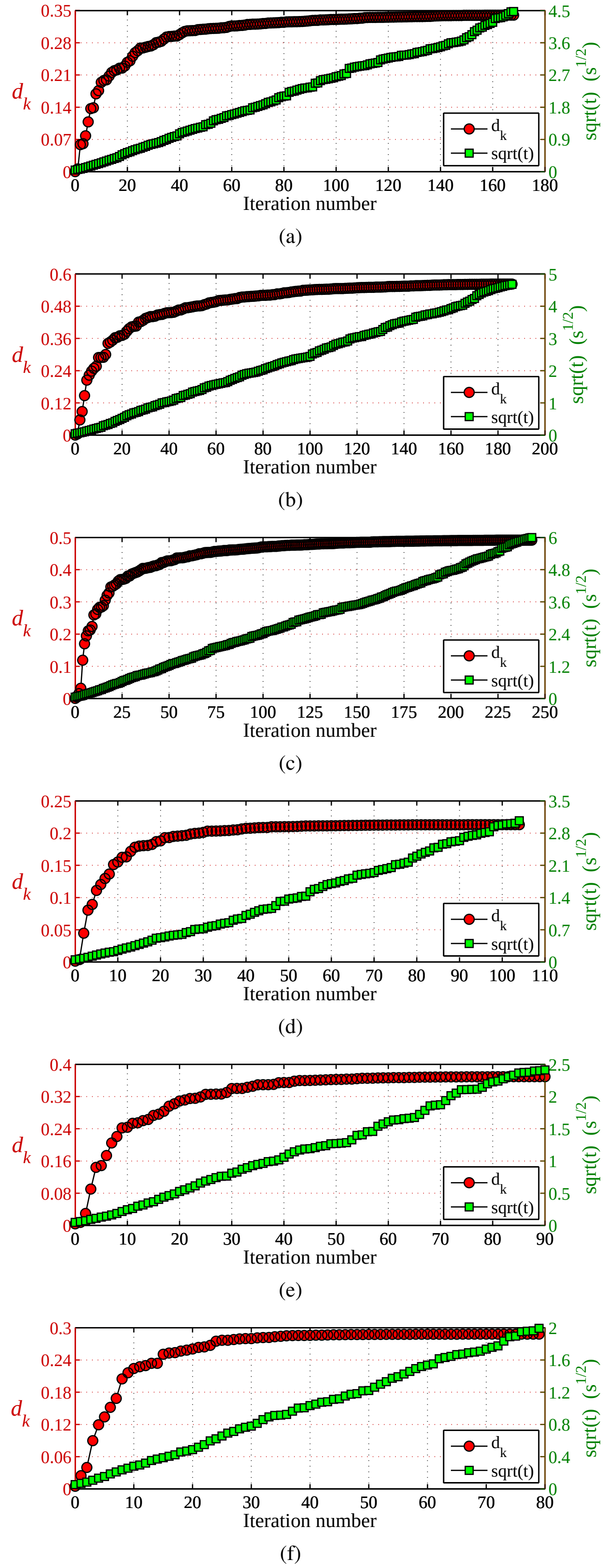

Fig. 4. The value d_k and the CPU running time t versus the number of iterations of our algorithm to compute (a)–(c) $d_Q(W)$ or (d)–(f) $d_Q(W^a)$ in the case of (b2), (e2), and (h).